Proceedings World Geothermal Congress 2005
Antalya, Turkey, 24-29 April 2005

Three-Dimensional Magnetotelluric Investigation in Geothermal Fields in Japan and Indonesia

Toshihiro Uchida

Geological Survey of Japan, AIST, Tsukuba 305-8567, Japan

uchida-toshihiro@aist.go.jp

Keywords: magnetotelluric method, 3D inversion, resistivity, geothermal reservoir, Ogiri, Japan, Mataloko, Flores, Indonesia.

ABSTRACT

A three-dimensional (3D) inversion code for magnetotelluric data has been developed and tested with field datasets obtained in several geothermal fields in Japan and Indonesia. The inversion code utilizes the least-squares inversion method with smoothness regularization. The forward modeling is by the finite difference method. Static shift, which is often an obstacle in the interpretation of MT data, is solved together with the underground resistivity structure in the inversion. A Bayesian criterion ABIC is applied to searching for the optimum trade-off among the minimization of the data misfit, model roughness and static shifts. The code has been successfully applied to the field data, showing sufficient stability, reliability and robustness in the computation. In this paper, 3D inversion results of the MT data obtained in the Ogiri geothermal field, southwestern Japan, and in the Mataloko geothermal field, eastern Indonesia, are presented. Recovered 3D resistivity models are generally similar to the two-dimensional (2D) inversion models, however, the deeper portion of the 3D model seems to be more realistic than that of the 2D model. The 3D models are also in a good agreement with the geological model of the geothermal reservoirs. These results indicate the necessity of the 3D interpretation for geothermal exploration and other application in complicated geological environments.

1. INTRODUCTION

The MT method is a major geophysical tool in geothermal exploration. Particularly, at an early stage of exploration, a resistivity model is key information to decide the location of pilot and production drillings. In such tasks, 2D inversion has been a standard technique for MT data interpretation in the past decade.

We often utilize TM-mode data for 2D interpretation of MT data in geothermal fields. It is mainly because we usually cannot achieve a good fitting for the TE-mode data by 2D inversion unless the subsurface structure is almost 2D. The TM-mode data can be easily explained by a 2D model, even if the real structure is 3D-like. However, the resultant 2D model may be unrealistic or contain false anomalies, although the final misfit of the TM-mode data can become small. Particularly, the resistivity model of deeper parts of the reservoir structure is often ambiguous.

To overcome such problems, 3D MT inversion techniques have been intensively studied in the past several years (e.g., Sasaki, 1999; Zhdanov et al., 2000; Mackie et al., 2001). Sasaki (1999, 2001) developed a 3D MT inversion technique and tested it with several synthetic datasets. Sasaki (2001) proposed to estimate static shifts simultaneously by the inversion. Uchida et al. (2002) applied the method to the MT data obtained in a geothermal field in Indonesia. In this work, the inversion code was slightly improved by incorporating more accurate Jacobian matrix and the optimal regularization for model-roughness minimization (Uchida and Sasaki, 2003).

2. 3D INVERSION METHOD

The 3D inversion scheme used in this work is based on the linearized iterative least-squares method with smoothness regularization (Sasaki, 1999). The forward modeling for a given arbitrary 3D earth is by the staggered grid finite difference method. For the modeling, the solution region, including both air and earth, is discretized into rectangular cells. The area of the solution region is wide enough as compared with the skin depth of the lowest frequency used for the inversion. The topography is not incorporated. The electric field is first solved in frequency domain by the finite difference method. Then, the magnetic field is computed from the obtained electric field.

The Jacobian matrix consisting of partial derivatives (sensitivities) of MT responses with respect to block resistivities in the 3D model should be evaluated from an estimated model at each iteration step in the usual iterative least-squares procedure. However, in this work, to save the computation time, the full sensitivities of the MT responses are computed at only a limited number of iterations; practically only at two iterations, for example, at the 3rd and 6th iterations. A Jacobian matrix computed from a homogeneous earth is used at the 1st and 2nd iterations. After the 3rd iteration, except the 6th iteration, the Broyden method is applied to updating the Jacobian matrix.

In addition to block resistivities of the 3D model, static shifts are also treated as unknowns in the inversion (Sasaki, 2001). A static shift is caused by shallow small inhomogeneities, and observed as a frequency-independent bias on apparent resistivity values, without changes in phase values. The amount of the shift is completely arbitrary and impossible to estimate from the observed apparent resistivity data. In this inversion, Gaussian-distributed static shifts are assumed. A regularization that the L-2 norm of static shifts is close to zero is applied.

To stabilize the model correction at each iteration step, smoothness regularization is adopted. The objective function U to be minimized in the inversion is defined as,

$$U = \left\| \mathbf{W}\left[\mathbf{d} - F(\mathbf{m}) - \mathbf{G}\mathbf{s}\right] \right\|^2 + \alpha^2 \left(\left\| \mathbf{C}\mathbf{m} \right\|^2 + \beta^2 \left\| \mathbf{s} \right\|^2 \right), \quad (1)$$

where $\mathbf{W}$ is the weight defined from observation errors, $\mathbf{d}$ is the observed data (apparent resistivity and phase), $\mathbf{m}$ is a 3D resistivity model, F is a non-linear function that works on the model $\mathbf{m}$ to produce MT responses, $\mathbf{C}$ is a roughening matrix, $\mathbf{s}$ is the static shift, and $\mathbf{G}$ is a matrix

that relates static shifts and the MT responses. The first term of the right-hand side is for the misfit minimization and second term is for roughness and static-shift minimization. α and β are trade-off parameters for roughness minimization and static-shift minimization, respectively, with regard to the misfit minimization.

An optimum regularization for the smoothness, α, and the static shift, β, is searched based on the ABIC minimization method at each iteration (Uchida, 1993). To reduce the search procedure, the optimum smoothness is searched every iteration except every 3rd iteration, while the optimum static shift is searched only every 3rd iteration, both by minimizing a Bayesian criterion ABIC.

3. MATALOKO GEOTHERMAL FIELD, INDONESIA

3.1 MT Data

Flores Island is located in eastern Indonesia. It is one of the numerous volcanic islands along the Sunda Island Arc, which spans almost the whole Indonesian country from west to east. The Mataloko geothermal field is located in the central part of the Flores Island (Figure 1). Figure 2 is a map of the Mataloko area, which is a vicinity of a local city Bajawa in central Flores. The survey area is on a highland, whose average elevation is approximately 1000 m. The area is underlain mostly by young volcanic formations (Muraoka et al., 2002). An active volcano, Mt. Inerie, is located in the west of the survey area. Also, there are numerous small volcanic cones that are younger than 0.5 Ma. We can recognize NW-SE and NE-SW trending lineaments of volcanic cones in the area. Three major surface geothermal manifestations, Mataloko, Bobo and Nage, are located in the studied area.

The MT survey was carried out in 1999 under a joint research work between the Indonesian and Japanese governments. The Geological Survey of Japan (GSJ) and New Energy and Industrial Technology Development Organization (NEDO) participated from Japan, and the Directorate of Mineral Resources Inventory (DMRI) joined from Indonesia.

The MT survey lines were arranged to cross the major trend of volcanic cones (Figure 2). Five NE-SW survey lines, Lines B-F, were arranged around the Mataloko manifestation zone. Two NW-SE survey lines, H and I, were set from the Bobo manifestation to the Nage manifestation zone. The total number of MT stations is 53; 41 on the Mataloko lines and 12 on the Bobo-Nage line. The station interval is approximately 600 m on the lines. The line spacing in the Mataloko area is approximately 500 m. A remote reference site was set up at the Mengeruda manifestation, which is approximately 15 km away north from the Mataloko area.

3.2 3D Interpretation

We applied the 3D inversion to the MT data at the Mataloko area. There were 39 MT sites used for the 3D inversion. Since the 3D inversion code currently utilizes the off-diagonal components of the impedance, Z_{xy} and Z_{yx} (apparent resistivity and phase), it may be important to choose an appropriate rotation direction. Therefore, two rotation directions were tested: 90 degrees (x-axis is east) and 45 degrees (x-axis is northeast). We refer to the former case as Case-1 and the latter as Case-2. Then, we carried out 3D inversion for each dataset with different mesh discretization in order to compare the effect of the rotation direction in the final models.

Twelve frequencies, from 0.03 Hz to 60 Hz, were used for the inversion. The size of the cells at the surface in the interpreted zone (shown by rectangles in Figure 2) was 200 m (or 125 m) horizontally and 100 m vertically. Gradually coarser cells were added outside the interpreted zone. The number of finite difference cells was approximately 50 - 60 in the x- and y- directions and 33 in the z-direction. The initial model was a homogeneous half space, whose resistivity was the average of the observed apparent resistivities. The underground resistivity structure was represented by numerous rectangle blocks whose resistivities were treated as unknown parameters in the inversion. The numbers of observed data was 1870, and the number of model parameters was 1900 for Case-1 and 1820 for Case-2. The MT responses used for the inversion were apparent resistivities in natural logarithmic domain and phases. For the weighting matrix $\mathbf{W}$, a noise floor of 1 % was assumed.

3D models obtained by the inversion for Case-1 and Case-2 are shown in Figures 3 and 4 as depth-slice sections. Figure 5 shows examples of MT responses on Line E. Figure 5a shows the pure 3D response from the model for Case-1 (Figure 3). There can be seen a gap between apparent resistivities of the two components, Z_{xy} and Z_{yx}, at high frequencies at Site 124. This gap caused by the static shift can be estimated by the inversion, and the curves that include the estimated static shifts fit the observed data well as shown in Figure 5b. The average of the estimated static shifts is approximately 0.5 in natural logarithm for both cases. This means that consideration of the static shift is necessary for the 3D inversion.

Although the data look different between the two rotation directions, Case-1 and Case-2, both data were well explained by individual inversions (Figures 5b and 5c). Also, the two models obtained by inversions for Case-1 and Case-2 are very consistent with each other in the interpreted zone (Figures 3 and 4), showing similar resistivity patterns in details on each depth slice. These results indicate that the rotation direction is not so crucial for 3D inversion even though we only used the off-diagonal components of the impedance. Of course, it would improve the model reliability more if we include all four components of the impedance in the inversion, particularly in a case when three-dimensionality is significant. However, it will be a theme of our future work.

When we compare the apparent resistivities of the Case-1 and Case-2, the splitting between the two components, Z_{xy} and Z_{yx}, at lower frequencies is bigger for Case-1 than Case-2 (Figure 5). It indicates that the major strike direction in the deep structure is either N-S or E-W. It is consistent with the shape of the high resistivity anomaly detected by the two 3D models in Figures 3 and 4. When we check the impedance skew in the original data, the skew values are generally small, less than 0.3, at many stations. There are, however, observed high skew values, greater than 0.3, at low frequency data at several stations in the northeastern part of the surveyed area. It means that three-dimensionality is not so significant in this field except the northeastern sites. It is the reason why a 3D shape high-resistivity basement (anomaly) was interpreted at the deep portion by the 3D inversion.

The western half of the deep model is characterized by a low-resistivity zone from a depth of 400 m to 1.5 km. When we assume an average resistivity of 1 - 2 ohm-m, this is consistent with the induction vectors at 0.3 Hz that point west or northwest directions (Uchida et al., 2002),

suggesting that the low resistivity body expands to this direction outside of the surveyed area.

We also conducted the 2D inversion for five lines, B-F (Figure 2). Shallow portions of the 2D models (Uchida et al., 2002) indicate similar resistivity patterns to those by the 3D inversion. However, probably due to the large skew at lower frequencies at northeastern stations, the 2D models indicate extremely high resistivity value in the deep resistive layer at the northeastern half of the lines.

Figure 6 shows a geological and geothermal interpretation of the 3D MT models. A surface alteration zone was recognized at the center of the Mataloko area by a geological survey (Figure 6, right-upper panel). The size of the alteration zone is relatively small on the surface; approximately 1 km in length along a small creek in the east-west direction. A geochemical survey revealed a high mercury concentration in the same zone, which is widely extending in the NE-SW direction (Tagomori et al., 2002). The surface low resistivity anomaly, which is extending in the east-west direction, is much wider than these two geological and geochemical features (Figure 6, right-upper panel). There seems to be a shallow hidden (not-outcropping) alteration zone that is widely surrounding the outcropping alteration anomaly. The hidden alteration zone must be overlain by a very thin high-resistivity layer, because even the highest frequency (60 Hz) data did not detect it but directly responded to the low-resistivity hidden alteration zone. The low-resistivity layer at depths between 200 m and 400 m widely spreads in the Mataloko area. Particularly, the very conductive zone, around 1 ohm-m, has a size of greater than 2 km in the east-west direction at a depth of 350 m (Figure 6, right-middle panel).

NEDO drilled two shallow exploration wells, MT-1 and MT-2, with a total depth of 207 m and 162 m, respectively, near the manifestation in Mataloko in the year 2000 (Sueyoshi et al., 2002). From the analysis of the cuttings, they recognized kaolinite and montmorillonite in volcanic rocks as major clay alteration minerals. The very conductive layer corresponds to the montmorillonite-rich zone, and it can be interpreted as the cap layer of the reservoir system. They also recognized wairakite from the bottom of the wells. It indicates that high-temperature hot water circulated up to this depth level. However, the thickness of the low-resistivity layer obtained by the 3D inversion is greater than 400 m near the drilling sites, and the thickness of the clay cap may also be a similar value. Therefore, the high-temperature hot water seems to have circulated upward through permeable fractures in the cap layer.

The high resistivity basement layer is widely distributed in the survey area. Its depth is shallower in the eastern half of the 3D model. In addition, a shallow anomaly of this resistive basement can be recognized slightly south of the manifestation zone (see depth sections at 300 - 800 m in Figure 4). A relatively resistive anomaly beneath a very conductive clay cap layer usually indicates a high-temperature water circulation zone. Hence, this resistive anomaly can be interpreted as the center of the geothermal reservoir system. Of course, it is not possible to identify the locations of the upflow zone of the geothermal circulation from the limited amount of survey data. Also, it is not easy to identify any fault structures or discontinuities in the high resistivity zone in the 3D resistivity model. However, we can say that this high-resistivity zone beneath the manifestation is a potential target of future development.

4. OGIRI GEOTHERMAL AREA, JAPAN

4.1 MT Data

The Ogiri geothermal area is located in a southern part of Kyushu Island, southwestern Japan (Figure 7). A 30-MWe geothermal power plant has been in operation by Nittetsu Kagoshima Geothermal Co., Ltd. (NKG) since 1996. The Shiramizugoe field, neighboring to Ogiri, is estimated to be a promising filed for future exploitation. The survey area is situated on a highland whose elevation is from 700 m to 900 m. The area is underlain by Quaternary volcanic rocks of a thickness of more than 2 km. Below this layer is a Mesozoic metamorphic formation that forms a basement layer of this region.

Three faults in an ENE-WSW direction have been identified in the survey area: Sakkogawa, Ginyu and Shiramizugoe from north to south (Figure 7). The major production zone of the Ogiri geothermal reservoir is associated with the Ginyu Fault (Goko, 2000). A new geothermal resource is under exploration by targeting the Shiramizugoe Fault. The geothermal reservoir in this area is distributed in the Quaternary volcanic layers that are mostly consisting of tuff and lava erupted from young volcanoes to the south and east of the area. The heat source of the current reservoir system is estimated to be the Kirishima volcano, which is an active volcano, a few kilometers to the east of the survey area.

NEDO, NKG and GSJ have conducted magnetotelluric surveys since 1996 over the Ogiri and Shiramizugoe geothermal fields at several stages. Intensive surveys were conducted by NEDO at Ogiri in 1999 for precise reservoir monitoring and at Shiramizugoe in 2000 for exploration of a new geothermal field. Several survey lines were set in the NW-SE direction so that they were perpendicular to the geologic strike, which was the direction of the faults. The spacing of the survey lines was 250 - 500 m. MT stations were basically arranged on the survey lines with an interval of 150 - 300 m. The MT stations therefore covered the two geothermal fields with a dense grid-like array. The number of MT stations used in this work is approximately 170. The remote reference analysis was applied to all the data with a reference site that was located approximately 40 km south from the survey area.

4.2 3D interpretation

For the 3D inversion, the MT impedance was rotated to the direction of the survey lines. Directions of *x*- and *y*-axes were 150 and 60 degrees clockwise from north, respectively. The numbers of MT stations and frequencies used for the inversion were 158 and 11 (from 0.0703 Hz to 72 Hz), respectively. Very noisy data whose observation error was greater than 200% were omitted before the inversion. Total number of observed data was 6912.

The cell size of the finite difference mesh in the interpreted zone (shown in Figure 7) was 150 m horizontally. The number of cells in the whole mesh was 68, 62 and 33 in *x*, *y* and *z* directions, respectively. Several cells were grouped into a resistivity block whose resistivity was dealt as an unknown parameter. The number of blocks in *x*, *y* and *z* directions was 18, 15 and 14, respectively. Therefore, the total number of resistivity blocks was 3780. The initial model was a homogeneous half space, whose resistivity was the average of the whole apparent resistivity data, which was 21 ohm-m.

Figure 8 shows depth-slice sections of the final 3D model at the 8th iteration. The normalized RMS misfit is 10.79, and

the average of the estimated static shifts is 0.744 in the natural logarithmic domain. Figure 9 shows the observed and calculated apparent resistivities and phases for the stations on Lines A and B. Fitting of the data is generally fine. Fitting for other stations is similar to that of Figure 9. Splitting of the two apparent resistivity curves below 1 Hz is not so large, but values of ρ*a-yx* are greater than ρ*a-xy* at most of the sites in this area. This feature indicates that these stations are located on a high-resistivity zone whose strike is close to *x*-axis. It is consistent with the resistivity structure deeper than 1.5 km in the 3D model in Figure 8.

The average of the estimated static shifts, 0.744, is relatively large. It is probably because of local topographic effects or complex changes of the surface resistivity. We can recognize large splits between the two apparent resistivity curves at higher frequencies at many sites. Also, there are large gaps in apparent resistivity between several neighboring sites. These shifts are well estimated by the inversion. Stations from 350 to 353 on Line-B are close to the production wells and the power plant. Therefore, the data quality of these stations is not good.

Resistivity structure of this area is characterized by a three-layer model: resistive first layer, conductive second layer and resistive third layer (Figure 8). Figure 10 shows a bird-eye view of the 3D model looked down from south. Shallow blocks down to a depth of 200 m are eliminated to compare the surface resistivity anomalies with the faults. Resistivity distribution of the shallow layers (less than a depth of 300 m) has a clear contrast between the high-resistivity zone in the northern half of the survey area and the low-resistivity zone in the southern half (Figure 8). At the mid depth, say from 400 m to 800 m, the whole area shows low resistivity. Then below a depth of about 800 m, high-resistivity anomalies are recognized at the center of the area, and they occupy the whole area at a depth of 2 km.

On the sections shallower than the 400 m depth, we can recognize the low-resistivity anomalies associated with the two faults, Ginyu and Shiramizugoe. As mentioned above, the low-resistivity anomaly is very wide around the Shiramizugoe Fault at the shallow depth. These can be interpreted as a zone of intensive clay alteration. The shallow high-resistivity zone in the northern side of the Sakkogawa Fault seems to be due to unaltered young lava layer. At a depth of about 1000 m, the resistivity structure is not consistent with the surface faults. The strike of this resistive anomaly is approximately NW-SE. We interpret the higher resistivity zones at the center of the survey area indicate the top of the geothermal reservoirs.

Figure 11 compare vertical sections of the 3D model along Lines A and B with 2D inversion results of TM-mode data. For Line-A, 2D and 3D models are very consistent with each other over the whole sections (Figure 11a). For Line-B, the upper boundary of the low-resistivity layer is similar between the 2D and 3D models. However, the lower boundary of the low-resistivity layer is different (Figure 11b). The 3D model shows a smoother boundary, while the 2D model shows that the low-resistivity anomaly continues to deep at the Sakkogawa and Ginyu Faults and at the Shiramizugoe Fault. These may be false anomalies caused by TM-mode data that is insensitive to deep structure. In this sense, the 3D model is more realistic than the 2D models.

Figure 12 shows a simplified geologic section estimated from the drilling data in the Ogiri geothermal field (NEDO, 2000). The Mesozoic basement layer is situated at a depth of about 2.5 km. Above it are Quaternary volcanic layers. The Ogiri geothermal reservoir is associated with the Ginyu Fault and located in the Quaternary volcanic layers. The temperature contours of 200 and 225 degrees Celsius indicate high-temperature anomalies beneath the Ginyu and Shiramizugoe Faults. The clay cap, in which low-temperature clay mineral such as smectite is dominant, is distributed in a zone whose temperature is below 200 degrees Celsius. Shapes of the lower boundary of the clay cap and the contour of 200 degrees Celsius are not only consistent with each other, but also consistent with the boundary between the conductive second layer and the resistive third layer in the vertical resistivity sections of the 3D model (Figure 11). The Ogiri production zone is located in the high-resistivity and high-temperature anomaly in the left-hande side (x = 2 km in Figure. 11) of the sections of the 3D model. A new production zone of the Shiramizugoe reservoir has been found by NEDO's pilot drillings targeting the high-resistivity and high-temperature anomaly in the right hand side (x = 4 km).

There are more than ten survey wells drilled by NEDO in the study area from which resistivity logging data is available (NEDO, pers. com.). Figure 13 compares resistivity logging data in five pilot wells in the Shiramizugoe field drilled in 2000 and 2001 with the corresponding blocks of the 3D model. Temperature logging data in two wells are also shown.

As for the logging data in the well SZ-1, which was drilled in the southern margin of the field, resistivity is very low at the shallow part and it increases as the depth increases. This resistivity profile is very consistent with the 3D model. The logging data in the other four wells (SZ-2 - SZ-5) show good agreement with the 3D model at depths deeper than about 600 m. However, the 3D model at shallow depths, from 200 m to 600 m, has lower resistivity than the logging data. Resistivity of the shallow zone may change rapidly in the horizontal direction, and some of these deviations might be explained by static shifts in the inversion. This is one possible reason why the very low resistivity layer was obtained by the 3D inversion.

The temperature data in the wells SZ-3 and SZ-5 show a high gradient at a depth range from 400 m to 800 m, indicating a zone of thermal conduction. Smectite was identified by X-ray analysis of the cuttings at this depth range in both wells. Temperature at depths over 800 m is almost constant between 200 and 250 degrees Celsius, indicating a hydrothermal convection zone. Smectite was missing in this zone, but chlorite and illite were identified by the X-ray analysis. From these comparisons, we can understand that the low-resistivity zone corresponds to the thermal conduction zone and the clay cap of the reservoir. On the other hand, the resistive third layer indicates the convection zone of high temperature, as explained in Figure 12.

5. CONCLUSIONS

A 3D inversion technique based on the finite-difference forward modeling and the least-squares inversion scheme with smoothness regularization has been developed and applied successfully to several field datasets. Static shifts were solved simultaneously in the inversion. The optimum trade-off with regard to the roughness minimization and the static shift minimization was determined by a Bayesian criterion ABIC. 3D interpretation of the Mataloko MT data has been performed in a stable manner. Applying the 3D inversion to two datasets of different rotation directions has revealed that the final 3D model does not depend on the

rotation direction significantly, even if we only use the off-diagonal components of the MT impedance for the inversion. However, it would be necessary to include all four components of the impedance in the inversion for obtaining more reliable 3D model in a case when three-dimensionality of the data is significant. The static shift seems to be estimated properly by our inversion.

The inversion scheme has also worked very well on a large volume MT field data obtained over the Ogiri and Shiramizugoe geothermal fields. 2D models beneath a few survey lines in Ogiri generated ambiguous structure at the boundary between the low-resistivity second layer and the high-resistivity third layer. It implies a limitation of the 2D interpretation. On the other hand, the 3D model seems to be more realistic for the entire resistivity model. Based on these experiences, it can be concluded that the 2D inversion is often insufficient in geothermal exploration, particularly in a complicated geological environment, and that the 3D interpretation is essential for geothermal exploration.

ACKNOWLEDGMENTS

The author thanks Dr. Yutaka Sasaki, Kyushu University, for providing the original 3D MT inversion code, and NEDO and NKG for giving permission to use the MT field data and logging data at Ogiri and Shiramizugoe fields for this study. The MT data in the Mataloko geothermal field was obtained jointly among DMRI, NEDO and GSJ under a project, "Research Cooperation Project on the Exploration of Small-Scale Geothermal Resources in the Eastern Part of Indonesia."

REFERENCES

Goko, K.: Structure and hydrology of the Ogiri field, West Kirishima geothermal area, Kyushu, Japan, *Geothermics*, **29**, (2000), 127-149.

Mackie, R., Rodi, W., Watts, M. D.: 3-D magnetotelluric inversion for resource exploration, *Expanded Abstracts, Society of Exploration Geophysicists 71st Annual Meeting*, (2001), 1501-1504.

Muraoka, H., Nasution, A., Urai, M., Takahashi, M., and Takashima, I., simanjuntak, J., Sundhoro, H., Aswin, D., Nanlohy, F., Sitorus, K., Takahashi, H., and Koseki, T.: Tectonic, volcanic and stratigraphic geology of the Bajawa geothermal field, central Flores, Indonesia, *Bulletin of Geological Survey of Japan*, **53**, (2002), 109-138.

NEDO: FY 1999 Report, Study on Geothermal Resources Exploration Techniques, Development of Technology for Reservoir Mass and Heat Flow Characterization, Electrical and Electromagnetic Monitoring (in Japanese), (2000)

Sasaki, Y.: 3-D inversion of electrical and electromagnetic data on PC, *Proceedings of 2nd International Symposium on Three-Dimensional Electromagnetics*, (1999), 128-131.

Sasaki, Y.: Three-dimensional inversion of static-shifted magnetotelluric data, *Proceedings of 5th SEGJ International Symposium*, (2001), 185-190.

Sueyoshi, Y., Matsuda, K., Shimoike, T., Koseki, T., Takahashi, H., Futagoishi, M., Sitorus, K., and Simanjuntak, J.: Exploratory well drilling and discharge test of wells MT-1 and MT-2 in Mataloko geothermal field, Flores, Indonesia, *Bulletin of Geological Survey of Japan*, **53**, (2002), 307-321.

Tagomori, K., Saito, H., Koseki, T., Takahashi, H., Dwipa, S., and Futagoishi, M.: Geology and hydrothermal alterations, and those correlations to physical properties obtained from gravity and resistivity measurements in Mataloko geothermal field, *Bulletin of Geological Survey of Japan*, **53**, (2002), 365-374.

Uchida, T.: Smooth 2-D inversion for magnetotelluric data based on statistical criterion ABIC, *Journal of Geomagnetism and Geoelectricity*, **45**, (1993), 841-858.

Uchida, T., Lee, T. J., Honda, M., Ashari, and Andan, A.: 2-D and 3-D interpretation of magnetotelluric data in the Bajawa geothermal field, central Flores, Indonesia, *Bulletin of Geological Survey of Japan*, **53**, (2002), 265-283.

Uchida, T., and Sasaki, Y.: Stable 3-D inversion of MT data and its application to geothermal exploration: *in* Macnae, J. and Liu, G. (eds.), *Three-Dimensional Electromagnetics III*, ASEG, (2003), 1-10.

Zhdanov M. S., Fang, S., and Hursin, G.: Electromagnetic inversion using quasi-linear approximation, *Geophysics*, **65**, (2000), 1501-1513.

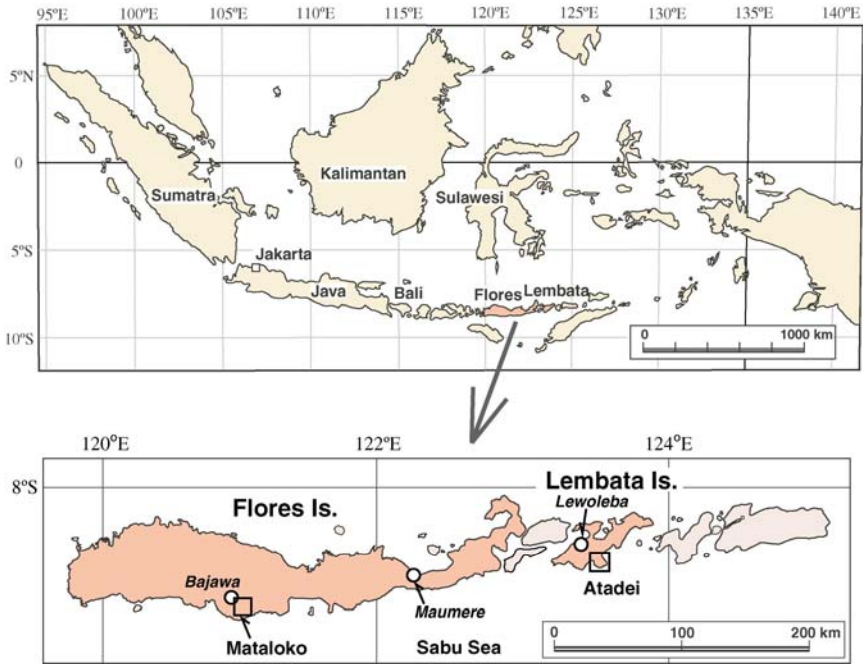

Figure 1: Location of the Mataloko geothermal field, Flores Island, eastern Indonesia.

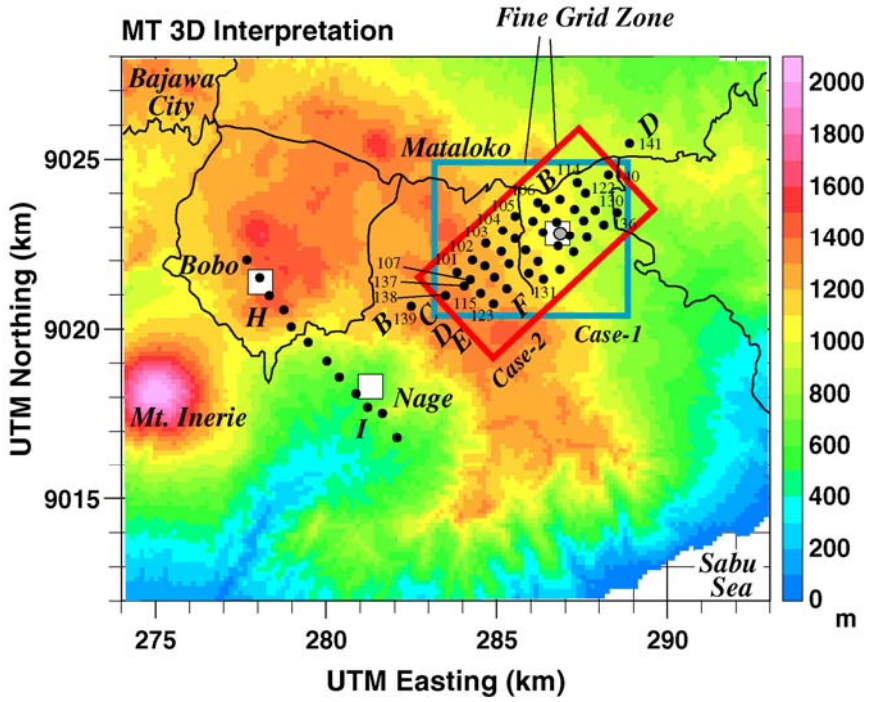

Figure 2: MT stations (black dots) in the Mataloko geothermal field plotted on a topography contours. Station numbers are shown for several MT sites. White squares indicate major surface manifestations. Gray circle is the drilling site at Mataloko. Thin solid lines are major local roads. Large rectangles indicate the zones for 3D interpretation: Case-1 and Case-2.

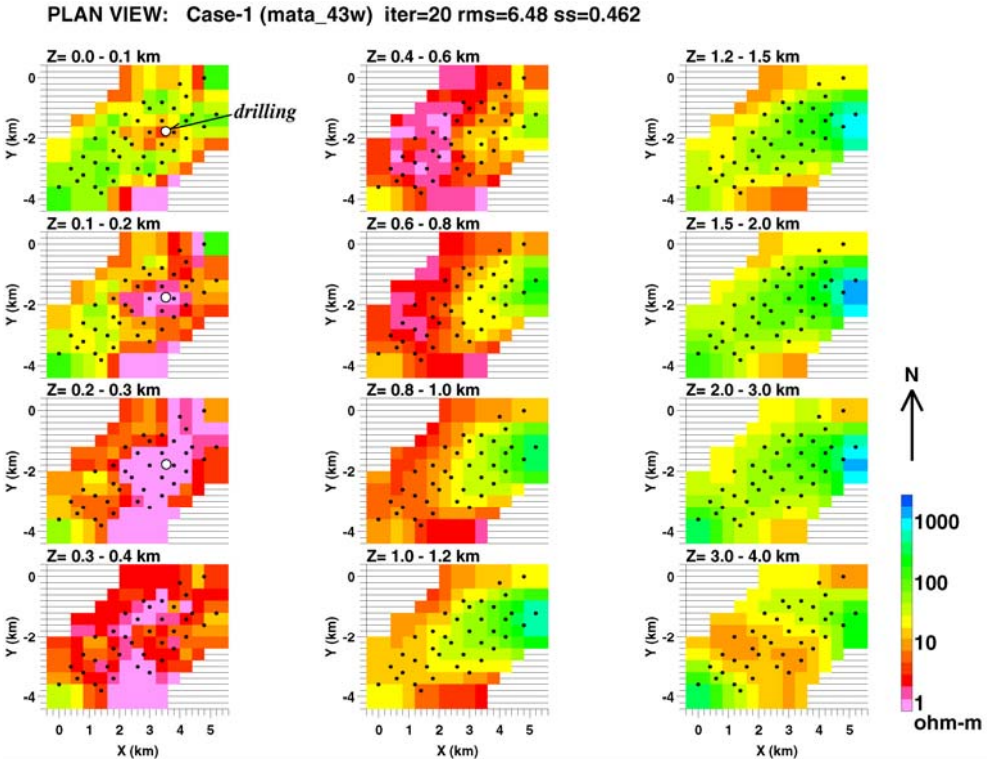

Figure 3: Depth-slice resistivity sections of the 3D model of Mataloko MT data for Case-1. Upper-left panel shows the shallowest section, and lower and right panels are deeper sections. Black dots indicate the MT sites. White circles on the three shallowest panels indicate the drilling site.

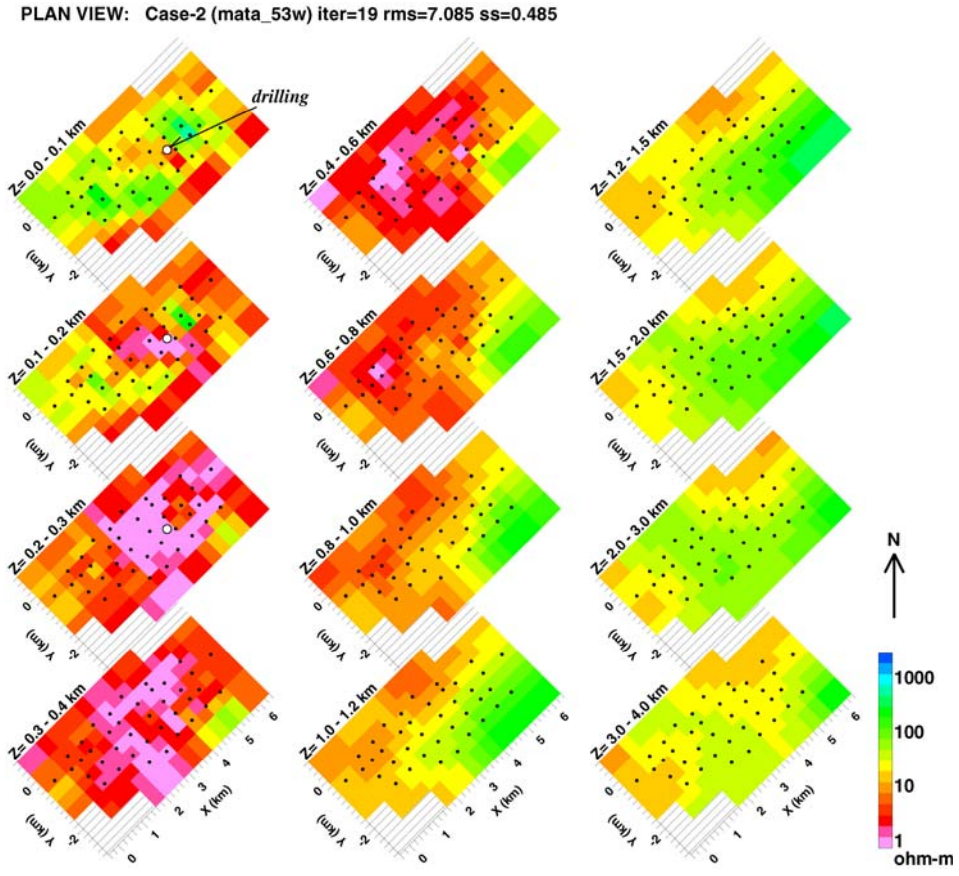

Figure 4: Depth-slice resistivity sections of the 3D model of Mataloko MT data for Case-2.

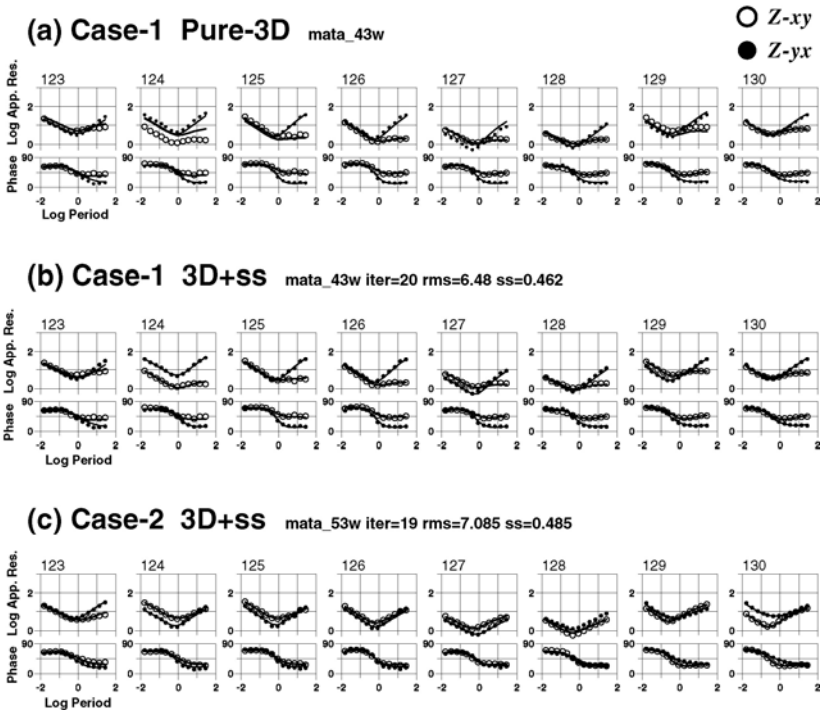

Figure 5: Examples of 3D responses (apparent resistivity and phase) on Line E in Mataloko. Circles are observed data, and lines are computed data. Open circles are the *xy*-components and solid circles are *yx*-components. (a) pure 3D responses for Case-1 (Figure 3), (b) 3D responses and static shifts combined for Case-1, and (c) 3D responses and static shifts combined for Case-2 (Figure 4). Error bars are not shown in these panels, although they were used as the weight of each data in the inversion.

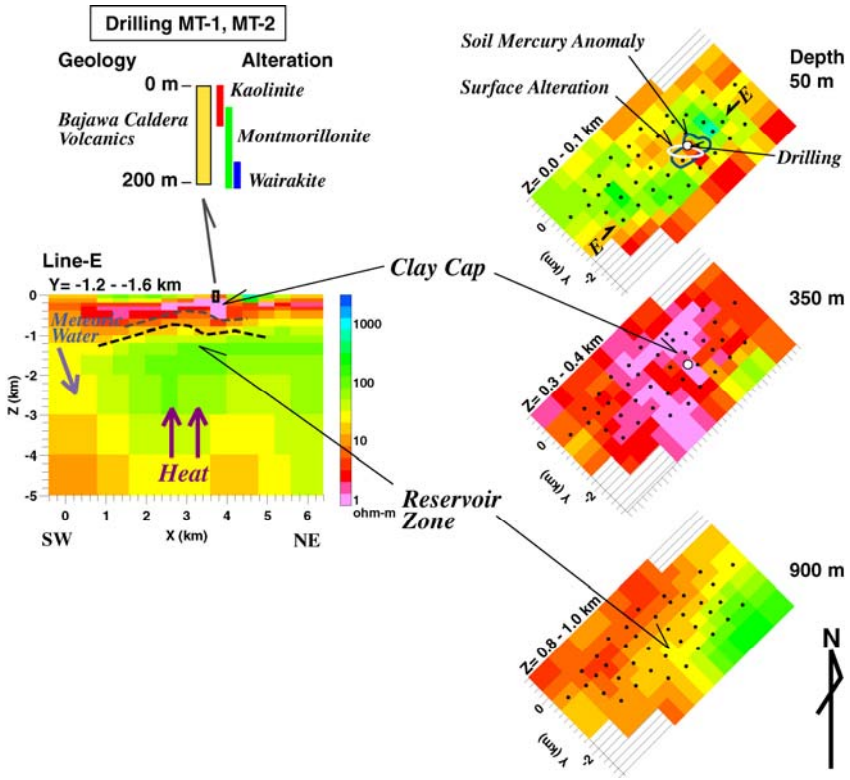

Figure 6: Interpretation of 3D resistivity model for the geothermal reservoir in the Mataloko area. One cross-section along Line-E (left) and three depth-slice sections (right) are shown. Zones of surface alteration and soil mercury anomalies greater than 2.4 ng/cm^3 are shown in the right-upper panel (Tagomori et al., 2002). Drilling data for wells MT-1 and MT-2 are also shown in the upper-left panel (Sueyoshi et al., 2002).

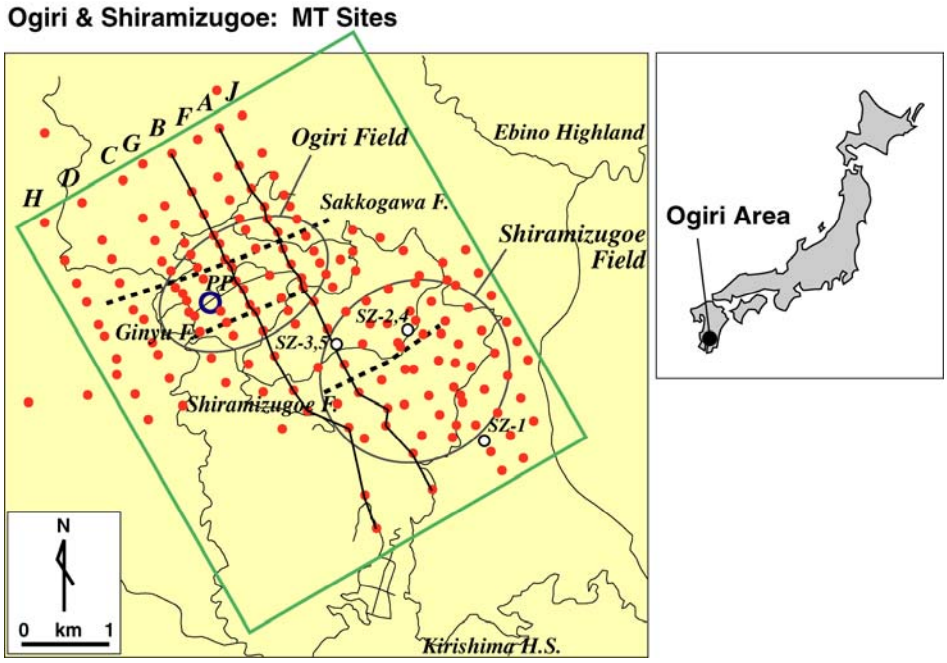

Figure 7: MT stations over the Ogiri and Shiramizugoe geothermal fields, southwestern Japan. Dots are MT stations, small open circles are pilot drillings, the large open circle with the letters PP is the Ogiri power plant, large ovals indicate centers of two geothermal fields, dashed lines are estimated faults, and thin solid lines are local roads. Letters A-H indicate names of the NW-SE survey lines. Lines A and B are shown with thick solid lines. The large rectangle indicates the region of 3D interpretation.

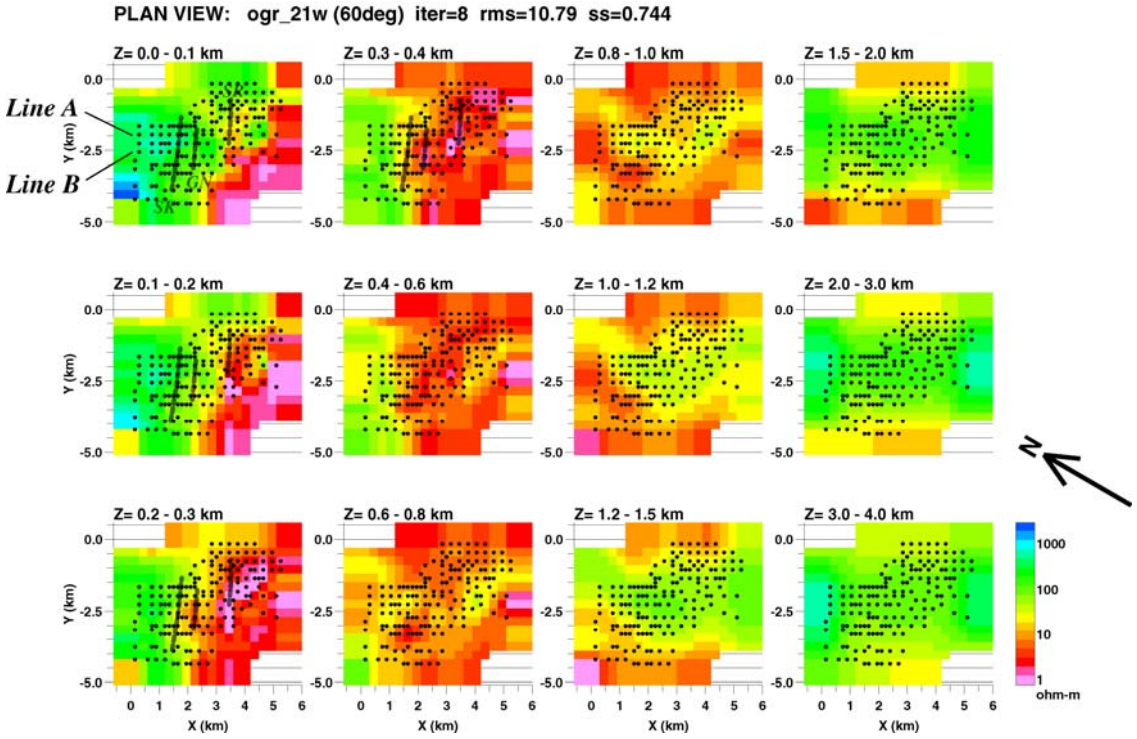

Figure 8: Depth-slice resistivity sections of the 3D model. The *x*-direction is 150 degrees clockwise from north. Black dots indicate the MT sites. Gray dashed lines on the four shallowest sections are location of estimated faults.

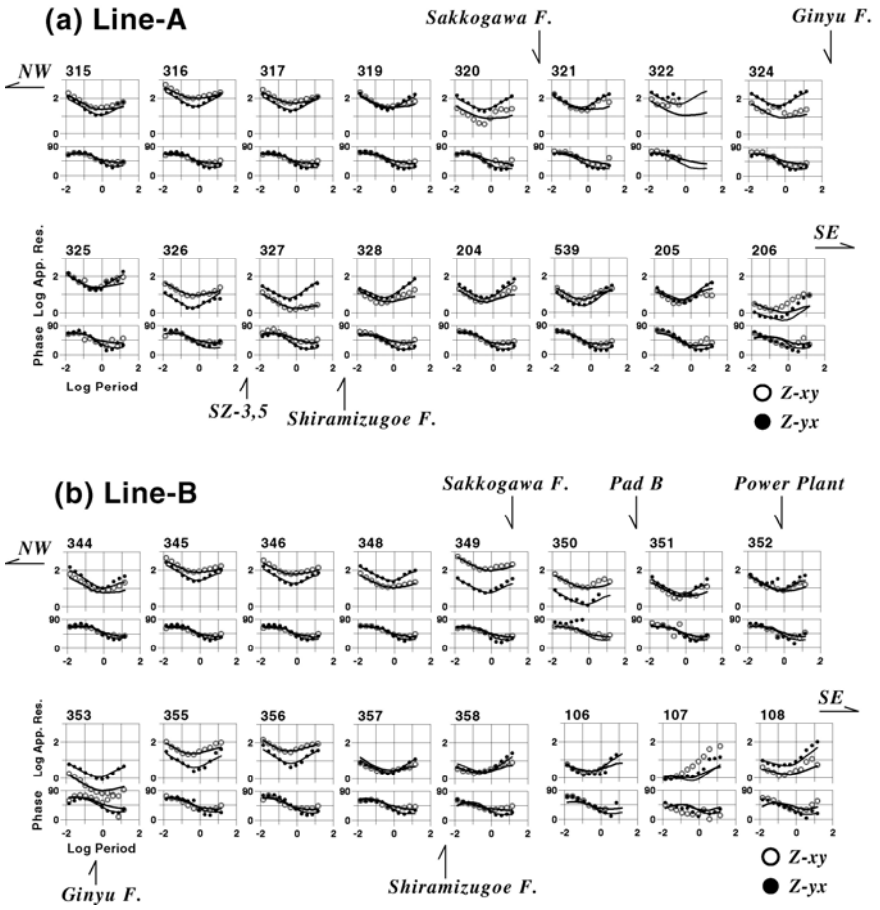

Figure 9: Observed (circles) and computed (solid lines) apparent resistivities and phases of the sites on (a) Line-A and (b) Line-B. Static shifts are included in the computed apparent resistivity curves.

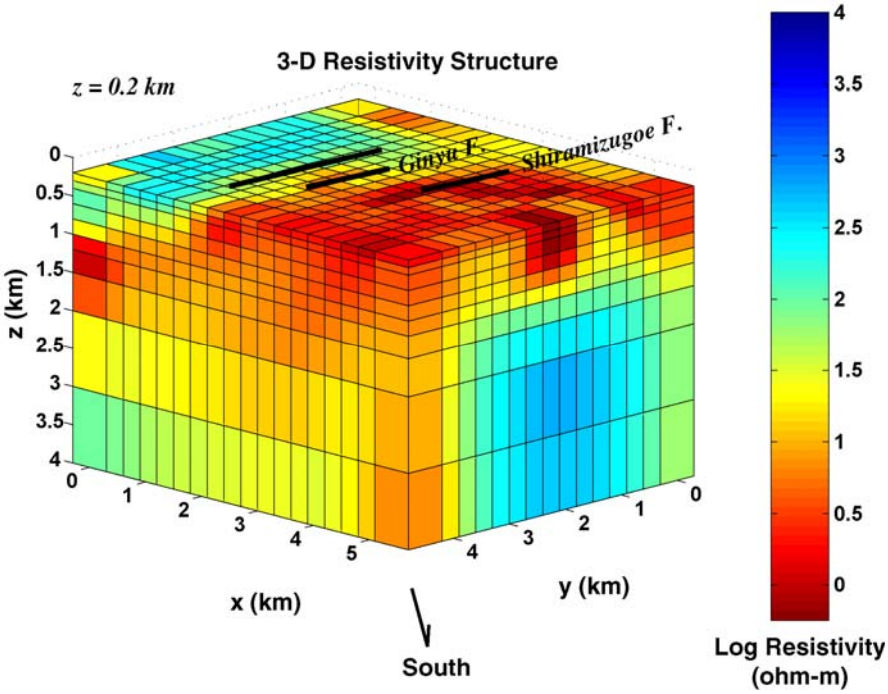

Figure 10: 3D view of the resistivity model from south. Shallow blocks to a 200m depth are stripped out and approximate locations of three faults are overlaid.

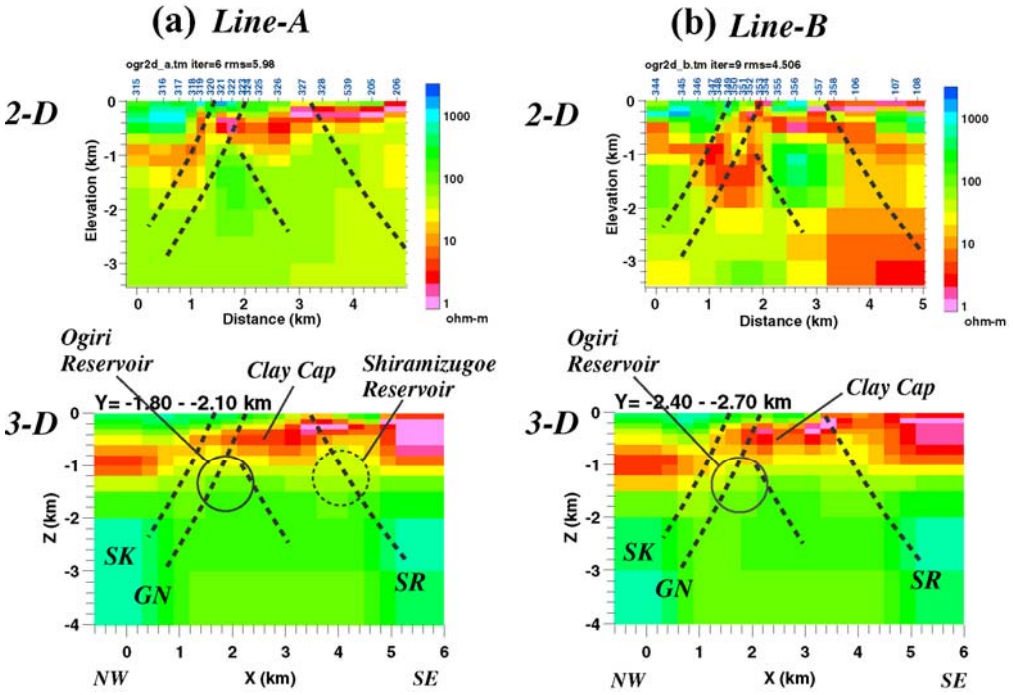

Figure 11: Comparison of 2D and 3D models along (a) Line-A and (b) Line-B. The 2D models (upper panels) are from the inversion of TM-mode MT data. The lower panels are vertical sections from the 3D model shown in Figure 8. Thick dashed lines are estimated faults. Large circles are estimated location of the production zones.

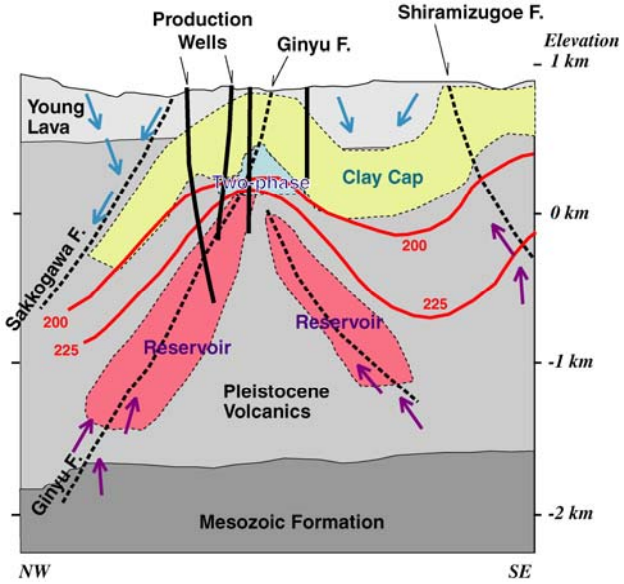

Figure 12: A simplified geology section along a NE-SW line around Lines A and B (reproduced from NEDO (2000)). Thick solid lines are several pilot and production wells. Red contours with numbers are temperature with values in degrees Celsius. Thick black dashed lines indicate faults; thin dashed lines are estimated outlines of the reservoirs and clay cap. Arrows indicate estimated cold and hot water flows.

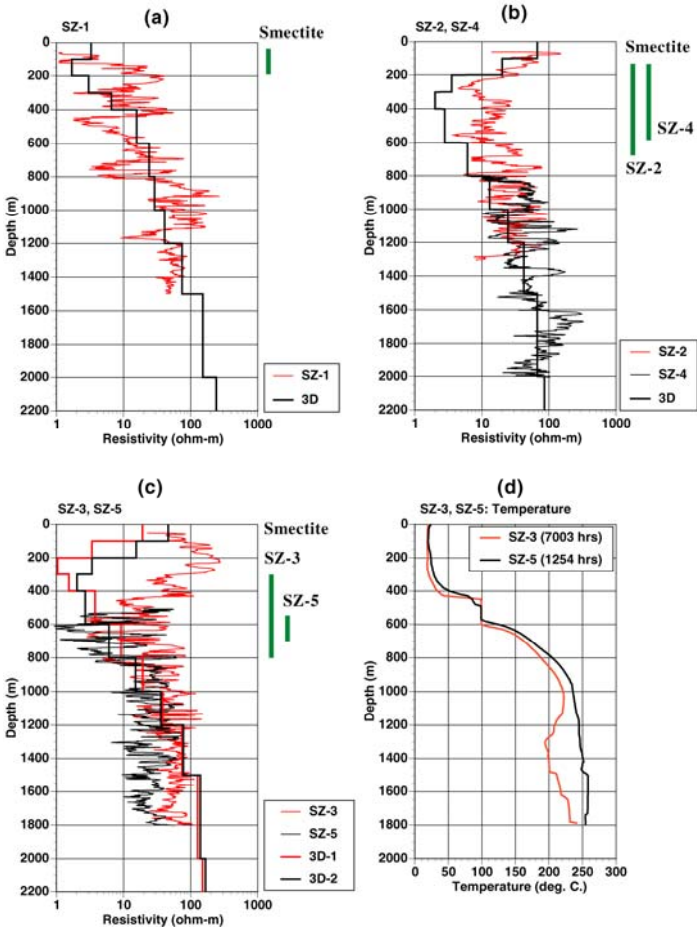

Figure 13: Comparison of resistivity logging data (thin black and red lines: long-normal array) with the 3D model (thick step-like lines) for (a) Well SZ-1, (b) Wells SZ-2 and SZ-4, and (c) Well SZ-3 and SZ-5. Panel (d) shows temperature logging data in Wells SZ-3 and SZ-5 at long standing times. Short vertical green bars on the right hand side of each panel indicate the zones where smecite was identified from the X-ray analysis of the cuttings.